Journal of Energy Storage 86 (2024) 111203

Contents lists available at ScienceDirect

Journal of Energy Storage

journal homepage: www.elsevier.com/locate/est

Research papers

Use of molten salts tanks for seasonal thermal energy storage for high penetration of renewable energies in the grid

Cristina Prieto [a,*], Pablo D. Tagle-Salazar [a,b], David Patiño [c], Julieta Schallenberg-Rodriguez [d], Padraig Lyons [e], Luisa F. Cabeza [b]

[a] Department of Energy Engineering, Universidad de Sevilla, 41092 Sevilla, Spain
[b] GREiA Research Group, Universitat de Lleida, Pere de Cabrera s/n, 25001 Lleida, Spain
[c] Department of Economics and Economic History, University of Sevilla, Avda. Ramón y Cajal, S/N, 41018 Seville, Spain
[d] Group for the Research in Renewable Energy Systems, Universidad de Las Palmas de Gran Canaria, Spain
[e] Tyndall National Institute, International Energy Research Centre, T12 R5CP, Ireland

ARTICLE INFO

Keywords:
Seasonal energy storage
Two-tanks molten salts system
Performance
Heat losses

ABSTRACT

Energy storage is acknowledged a key technology to meet the challenges posed by the energy transition. Short-term grid-connected storage, based on Li-Ion batteries, is becoming commonplace but seasonal energy storage at grid-scale will be needed for deep decarbonisation of the electrical power system. Pumped hydropower is considered to be the only mature technology for such applications, but this paper demonstrates that two-tanks molten salts systems, that are used today in commercial concentrating solar power (CSP) plants, can also be considered a mature technology that can be used at large scale for seasonal energy storage. This was established by evaluating the annual heat losses of molten salts tanks using validated models of these systems. The results show that the heat losses in a very well insulated molten salts tanks are around 1 K/day, which would result in good economic performance of the power block even if storage was required for up to months.

1. Introduction

An energy transition (or energy system transformation) is a significant structural change in an energy system regarding supply and consumption, therefore it goes beyond small changes or punctual changes. According to IRENA [1], the success of the low carbon energy transition will depend on a transformation of the global energy sector from fossil-based to zero-carbon sources by the second half of this century, reducing energy-related CO_2 emissions to mitigate climate change and limit global temperature to within 1.5 °C of pre-industrial levels. They have developed a pathway to achieve a 36.9 Gt reduction in CO_2 that requires six technological avenues, 25 % of the reduction would come from new renewable sources, 25 % from energy efficiency actions, 20 % from electrification, 10 % from hydrogen use, 6 % from fossil fuels CO_2 capture and storage (CCS), and 14 % from renewable energy-based CO_2 removals (BECCS).

According to the International Energy Agency (IEA) [2], over the decade 2010–2020, the renewable based electrical energy generation grew worldwide from 6213 TWh in 2010 to 9506 TWh in 2020. Much of this growth (Fig. 1) comes from solar PV (+96.18 %), wind (+78.70 %), and other renewables (+46.49 %).

Renewable electricity generation, particularly PV and wind, are variable and dependent on weather conditions, necessitating the use of other forms of generation when they are not available. The current conventional approach to provide this generation is to use fossil fuels, in the form of coal, gas or oil-based generation, to provide energy when renewable energy production is limited. An alternative low-carbon approach is to store excess renewables-based production, using grid-scale energy storage, and release it to the electricity system when renewable production is limited.

According to the IEA [3], pumped-storage hydropower is the most common form of energy storage both in terms of installed capacity and energy stored. In pumped-storage, water is pumped into a reservoir and then released to generate electricity at a different time, but this can only be done in certain locations.

Batteries, typically Lithium Ion (LiIon) are now playing a growing role in the provision of grid-scale energy storage, as they can be installed anywhere in a wide range of power and energy levels and are becoming very popular worldwide to provide services to electricity system operators to provide grid services. Furthermore, while batteries can cost effectively provide significant amounts of power and are thus very useful

* Corresponding author.
E-mail address: cprieto@us.es (C. Prieto).

https://doi.org/10.1016/j.est.2024.111203
Received 5 December 2023; Received in revised form 13 February 2024; Accepted 28 February 2024
Available online 8 March 2024

Nomenclature

General symbols

A	Surface area (m^2)
C_p	Specific heat capacity (J/kg·K)
DHI	Diffuse Horizontal Irradiation (W/m^2)
DNI	Direct Normal Irradiation (W/m^2)
GHI	Global Horizontal Irradiation (W/m^2)
h	Specific enthalpy (J/kg)
m	Fluid mass (kg)
$\dot{m}$	Mass flow (kg/s)
q	Heat flow (W)
q_T	Total heat loss (W)
S	Cooling rate (K/day)
T	Temperature (°C)
u	Specific internal energy (J/kg)
V_{MS}	Volume of salt inventory (m^3)

Greek letters

α_s	Solar absorptance of surface
θ_{alt}	Solar altitudes (rad)
μ	Dynamic viscosity (Pa·s)
ρ	Density (kg/m^3)
ρ_{ground}	Reflectance of the ground surface

Subscript

CC	Combined (mixed) convection
G	Gas
jac	Jacket
MS	Molten salts
NC	Natural convection
rad	Radiation

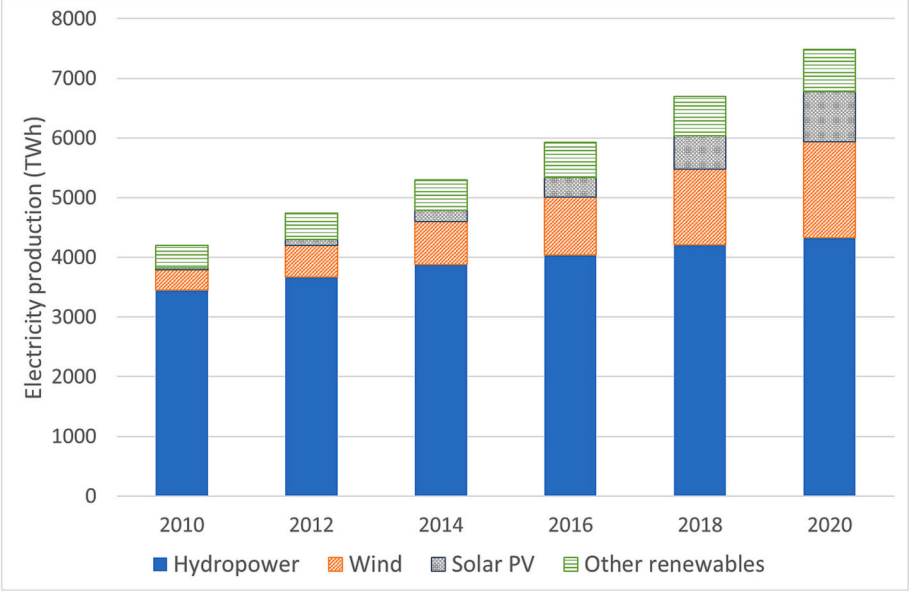

Fig. 1. Worldwide electricity production from renewable energy sources. Data source: [2].

for the provision of short-term frequency regulation services, the amount of energy that can be cost effectively stored in batteries is relatively small. Furthermore, while battery costs have fallen dramatically in recent years due to the scaling up of electric vehicle production, market disruptions and competition from electric vehicle makers have led to rising costs for key minerals used in battery production, notably lithium. It is now becoming evident that further cost reductions rely not just on technological innovation, but also on the prices of battery minerals. Therefore, there are significant economic limitations in their application beyond providing 2 h of storage.

Authors such as Bahlawan et al. [4] highlight the need of longer-duration or even seasonal energy storage at grid-scale to reduce the need for fossil-fuel based generation. To provide longer duration grid-scale storage, a number of other technologies are under consideration including compressed air energy storage (CAES), Liquid Air Energy Storage (LAES) and Hydrogen Storage (HS) which are not commercially mature or technology thermal energy storage (TES) based in two-tanks solar salt storage which is regarded a much more mature energy storage technology [5].

The two-tanks TES system is the most widespread storage system in CSP commercial applications due to its good thermal properties and reasonable cost [6]. Nowadays, molten salts provide a thermal energy storage solution for the two most mature technologies available on the market (e.g., parabolic trough and tower) and is used as direct and indirect storage depending on the selected plant philosophy (Fig. 2). According to IRENA [7], today there is 491 GWh of molten salts systems installed capacity currently that could grow to 631 GWh by 2030.

Molten salt storage in CSP plants has proven to be an effective solution for managing the daily intermittency of solar generation. However, it has never been considered for seasonal storage due to perceived limitations in terms of space, long-term thermal efficiency, maintenance costs, and restricted charge-discharge cycles. As longer duration / seasonal energy storage becomes more important, more suitable alternatives are being researched and developed to address this critical challenge in the transition to a more sustainable energy matrix [7–10]. Molten salts are a viable and promising option for seasonal energy storage due to their high storage capacity, thermal efficiency, design flexibility, accumulated expertise, and successful applications.

In this research, the significant potential for the use of molten salts based thermal energy storage technology for the provision of long-term

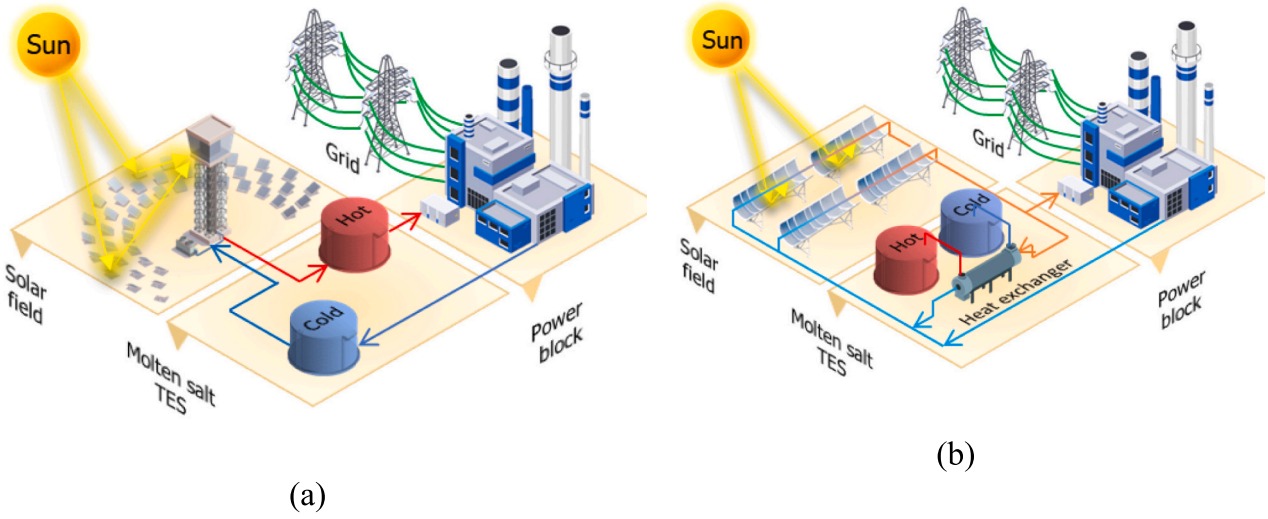

Fig. 2. Schematic flow diagram of a tower plant with 2-tank molten salt storage system. (a) Direct configuration, (b) Indirect configuration.

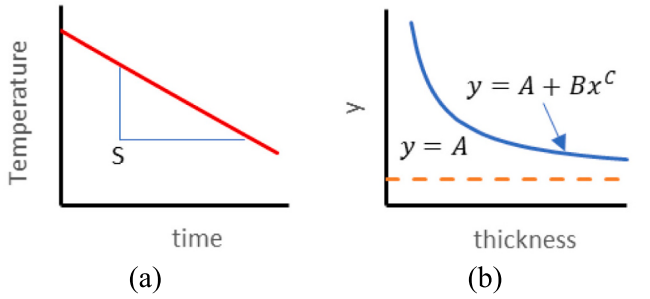

Fig. 3. Description of the methodology considered: (a) Calculation of cooling rate and (b) Estimation of the asymptote at y = A.

/ seasonal energy storage, in future low carbon electricity systems will be demonstrated.

2. Materials and method

2.1. Methodology

To evaluate if molten salts technology can be used for long-term grid-scale energy storage, an illustrative example, estimating the annual heat losses of molten salt tanks, using a detailed model of a system located in Seville, Spain was carried out. A sensitivity analysis of heat losses was done varying the mineral wool insulation thickness.

The heat losses will result in a drop of temperature during the period of storage with a given insulation thickness and a given climatology for Winter and Summer (cooling rate "S" in K/day, Figure a), and the error is calculated using Eq. (1). This parameter is intended to measure the difference between the results respect to the season.

$$Error = \frac{S_{winter} - S_{summer}}{S_{summer}} \bullet 100\% \quad (1)$$

Heat flow diminishes as insulation thickness increases, and it is expected to follow an asymptotic profile, as illustrated in Fig. 3b. Furthermore, it is expected that the cooling rate will also follow a similar asymptotic pattern concerning insulation thickness. As insulation thickness increases, it is assumed that the asymptote of heat flow through the insulation (walls and the top) should approach zero. However, this assumption does not hold for the heat flow through the floor, which exhibits distinct behaviour. The primary objective of this analysis is to estimate the coefficients A, B, and C of the asymptotic profile for both heat flows and the cooling rate.

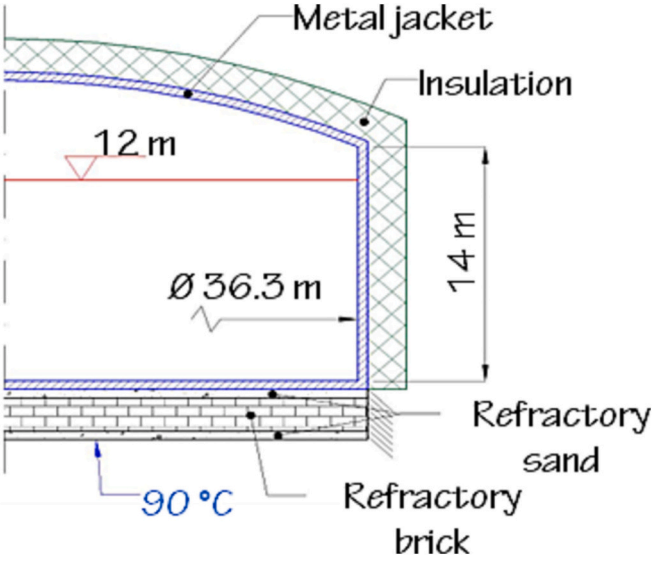

Fig. 4. Sketch of the molten salt tanks.

To achieve this estimation, a regression approach was employed, comparing heat flow and cooling rate against the insulation thickness. Coefficients A, B, and C are computed to maximize the coefficient of determination (R^2) of the regression, enabling a precise determination of the asymptotic characteristics in the context of heat flow and cooling rate behaviour as insulation thickness increases. Subsequently, the cooling rate will be represented by an equation, and the asymptote at y = A can be estimated (Fig. 3b) This parameter is used to determine the temperature drop needed to estimate the duration for which the tanks can retain energy with acceptable thermal losses for the economic performance of the full solar power plant.

2.2. Description of the storage tanks

Fig. 4 shows a sketch of the molten salt tank considered for this analysis. The steel wall used was stainless steel of 0.6 cm thickness for the bottom, 3.3 cm for the wall, and 0.7 cm for the top. The insulation considered was mineral wool for the walls and top, while the bottom

Table 1
Parameters of the materials.

Layer	Material	Density (kg/m^3)	Specific heat capacity (J/kg·K)	Thermal conductivity (W/m·K)
Steel wall[a]	Stainless steel	7850	554	$14.7 + 0.015 \cdot T$
Insulation[b]	Mineral wool	160	840	$0.037 + 2 \bullet 10^{-4} \cdot T$
Refractory sand[c]	Freeflow 1000 R	240	1008	$0.01825 + 3.225 \bullet 10^{-5} \cdot T + 3.125 \bullet 10^{-8} \cdot T^2$
Refractory brick[c]	Promasil 1100	300	1030	$0.07325 - 1.025 \bullet 10^{-5} \cdot T + 9.375 \bullet 10^{-8} \cdot T^2$

[a] Data obtained using Engineering Equation Solver (EES) material database.
[b] Data provided by [11].
[c] Data found in manufacturer's website.

Table 2
Thermophysical properties of the storage medium, solar salt [12].

Property	Value
Density (kg/m^3)	$\rho = 2090 - 0.636 \cdot T$
Dynamic viscosity (Pa•s)	$\mu = 22.714 \bullet 10^{-3} - 0.12 \bullet 10^{-3} T + 2.281 \bullet 10^{-7} T^2 - 1.474 \bullet 10^{-10} T^3$
Thermal conductivity (W/m·K)	$k = 0.443 + 1.9 \cdot 10^{-4} \cdot T$
Specific heat (J/kg·K)	$c_p = 1443 + 0.172 \cdot T$

insulation (which is considered fixed in simulations) was 2 cm of refractory sand Freeflow 1000 R and 30 cm of refractory brick Promasil 1100, insulation provided by Promat Ibérica S.A. The properties of the materials are detailed in Table 1. The storage medium used was a mixture of 60 wt% $NaNO_3$ and 40 wt% KNO_3, so-called "solar salt"; the thermophysical properties are presented in Table 2.

2.3. Weather conditions

Weather data used in this analysis correspond to data acquired in a weather station in Seville (Spain). The irradiation considered for a Direct Normal Irradiance exceeding 400 W/m2 in Summer was 8.25 kWh/m^2·day, and in Winter, 3.4 kWh/m^2·day. The weather conditions for Summer and Winter are shown in Fig. 5. Analysis reveals distinct probability functions characterizing temperatures and wind speeds during both summer and winter seasons. During summer, temperatures predominantly fall within the range of 22 °C to 38 °C, whereas in winter, they tend to hover between 9 °C and 17 °C. Wind speed exhibits a similar behaviour in both seasons, with a predominant value below 2.5 m per second. These findings underscore the significant seasonal variations in meteorological parameters, emphasizing the need for context-specific analyses when addressing temperature and wind-related influence on heat losses.

2.4. Description of the transient model for heat loss estimation

A detailed description of the mathematical model can be found in [13]. OpenModelica [14] was the software used for implementing the mathematical model, which is based on one-dimensional transient-state heat transfer. The storage media, the solar salts, and the cover gas were considered to be ideally mixed and single-phase fluids with uniform temperature distribution. The model considers the flow of the storage media, the solar salts, and of the cover gas between the two storage tanks. Heat losses were modelled considering conduction, convection, and radiation according to the equations presented in Table 3. Inside the tank, the fluids transfer heat to the jacket casing via natural convection and radiation. The model also considers heat transfer due to solar radiation and mixed convection at the external surface of the tank. This model was specifically designed for CSP applications, where the HTF circulates into and out of the tank. To align with this application scenario, the mass flow of the HTF was intentionally set to zero for the purpose of this study.

A notable enhancement of the model used in this work is the inclusion of the effects of the local heat losses stemming from assembly defects that may manifest themselves in real-world scenarios. The estimation of these effects was based on real data from a pilot plant with 8.1 MWh_{th} thermal capacity that was available in Seville (Spain) [15] and another smaller pilot plant available in Lleida (Spain) [16], and is modelled with:

$$q_{local} = -12.14667 - 0.06962 T_{MS} + 49.33775 L + 3.71871 D \quad (2)$$

where q_{local} is the total heat flow by local effects (in kW), T_{ms} is the temperature of the salts inside the tank (in °C), L is the fraction level of salts (height of salts over tank height), and D is the diameter of the tank (in m).

The foundation of the tank typically includes a passive air-cooled layer for refrigeration purposes, designed to maintain a maximum temperature of 90 °C [17]. In this study, a fixed-temperature boundary condition was applied to simplify the analysis, as illustrated in Fig. 4. Subsequently, heat flow through the bottom is determined using a multi-layer conduction model, where the heat sump is a surface at a constant temperature of 90 °C.

3. Results and discussion

Fig. 6 presents the estimated heat losses through the wall and the top vs. the thickness of insulation. As mentioned above, the heat losses in the bottom are considered without varying the insulation thickness, where it was obtained an average heat flux of about 91.97 W/m^2. The heat loss in the walls and roof shows the expected asymptotic behaviour mentioned in Section 2.1. The heat losses through the walls and top do not vary significantly from Summer to Winter even when the weather conditions are very different, as shown in Section 2.3. Specifically, the heat loss through the walls decreases significantly, ranging from approximately 275 W/m^2 with 15 cm of insulation to merely 48 W/m^2 when 1 m of insulation is applied. Similarly, losses through the top of the tank demonstrate a closely aligned pattern, decreasing from around 193 W/m^2 with 15 cm of insulation to a mere 35 W/m^2 with 1 m of insulation.

Fig. 7 presents the estimated temperature drop from the tank with time for different insulation thicknesses. As it can be seen, the tanks would lose 2 K per day in a tank ideally built and 2.3 K per day in a tank with local losses when only 15 cm of insulation is considered. But when 45 cm of insulation would be used in the walls and top of the tank, these heat losses would decrease to 0.92 K and 1.24 K, respectively. Moreover, in both cases, the temperature drop reaches an asymptote with 1 m of insulation thickness (reasonable given the dimensions of the tanks), which mean a 0.3 % temperature drop and 0.45 % temperature drop, respectively. Moreover, in both cases, the error value remains minimal, measuring below 2 %. Consequently, it is reasonable to presume that the impact of weather fluctuations stemming from seasonal changes is negligible.

The total estimated temperature drop in the storage tanks after 1 month at 565 °C for different insulation thicknesses is shown in Table 4. Notably, there is a significant absence of significant temperature drop disparities between summer and winter results. In both seasons, the temperature drop exhibits similar values (due to low error in results). However, a significant shift in dynamics becomes evident when accounting for local heat losses. In scenarios where these losses are factored into the equation, a discernible difference of approximately 10 K becomes apparent when compared to scenarios where local losses are not considered. This divergence underscores the pivotal role played by local heat losses in shaping the thermal behaviour of the system,

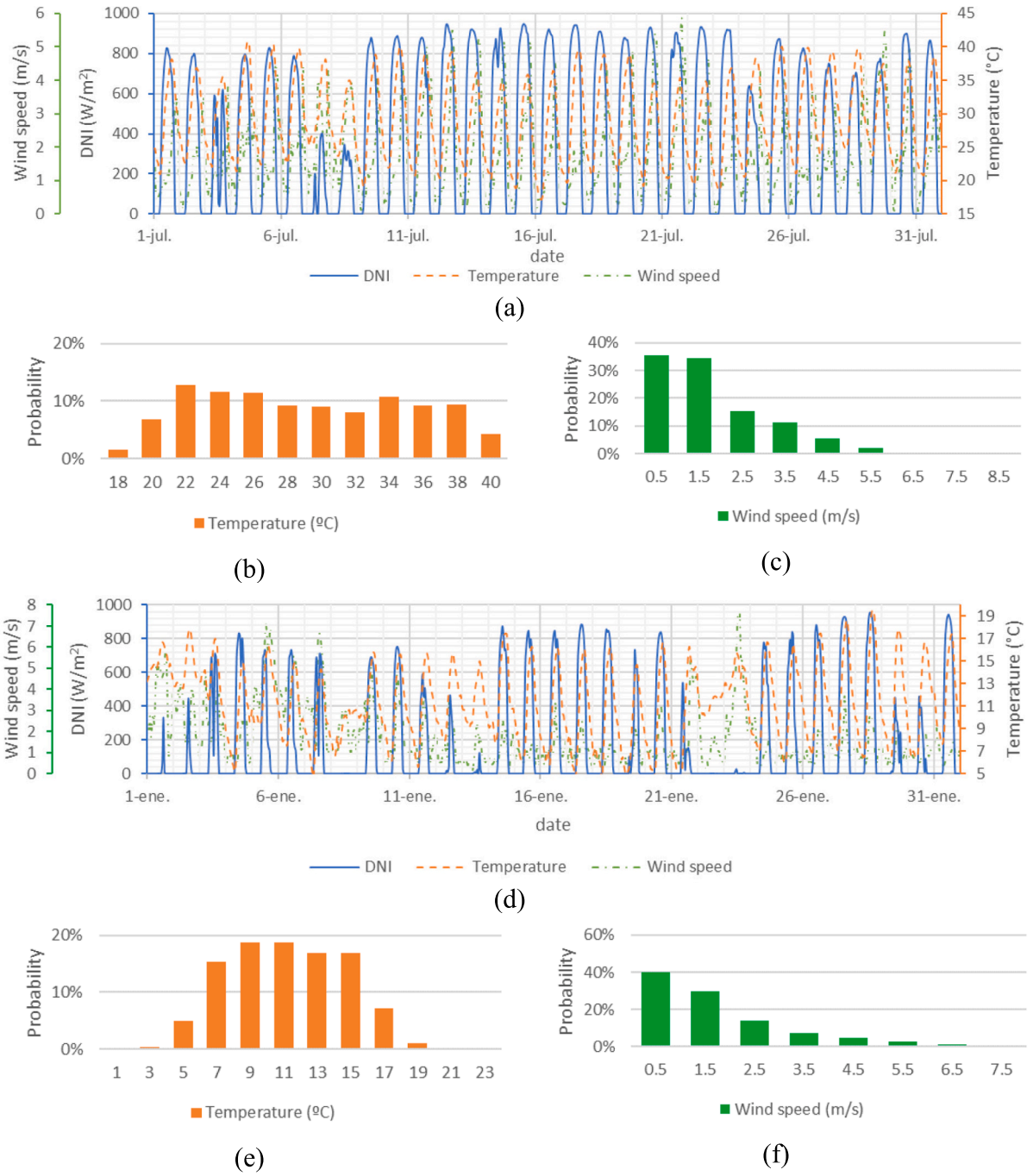

Fig. 5. Weather conditions considered. (a) Summer weather; (b) Summer temperature probability; (c) Summer wind velocity probability; (d) Winter weather; (e) Winter temperature probability; (f) Winter wind velocity probability.

introducing an additional layer of complexity to the otherwise seasonally consistent temperature patterns observed.

The results of the calculated coefficients A, B, C of thermal losses and the cooling rate are presented in Table 5. Based on the coefficient of determination (R^2), the heat flux at bottom has an asymptote at around 91.97 W/m^2, while the heat flux at the walls and top has a very low value of asymptote (or no asymptote). These results affirm the validity of the assumption regarding the zero-value asymptote of heat loss through walls and the roof. Furthermore, the coefficient of determination is higher when not considering the asymptote for this heat flow profiles. In the context of heat flow through the bottom surface, it is crucial to highlight the distinctiveness of coefficient B in comparison to heat flow through other surfaces. The remarkable feature of coefficient B is its near-zero absolute value, which signifies an almost-constant trend. This characteristic allows for the consideration of this heat flow as exhibiting a nearly constant behaviour. Fig. 8 shows that most of the heat losses come from salts (≈98 %). The remainder heat losses are from the jacket layers and the cover gas (≈2 %). Moreover, local losses represent about 32.07 ± 8.38 % of the total losses. And finally, the share of losses tends to be similar independently of the weather conditions or insulation thickness.

Table 5 shows that the cooling rate has an asymptote at 0.21 K/day when local heat losses are not considered and at 0.53 K/day when they are considered. These values represent the minimum achievable cooling rate when dealing with infinite thickness ($t \to \infty$) or perfect insulation ($k \to 0$). It is worth noting that this value may vary with the size of the

Table 3
Summary of the energy and mass balances in model used [13].

Heat flow	Description
Energy balance of the molten salt	$\frac{d(m_{MS}C_pT)}{dt} = \dot{m}_{in}h_{in} - \dot{m}_{out}h_{out} - q_{T,MS} + q_{reh}$
Mass balance of the molten salt	$\frac{dm_{MS}}{dt} = \dot{m}_{in} - \dot{m}_{out}$
Energy balance of the cover gas	$\frac{d(m_G u)}{dt} = \dot{m}_G h_G - q_{T,G}$
Mass balance of the cover gas	$\frac{dm_G}{dt} = \dot{m}_G = -\rho_G\left(\frac{dV_{MS}}{dt}\right)$
Energy balance in the interface surface	$q_{NC,MS} = q_{NC,G} + q_{rad,G}$
Heat flows to the jacket layers in surfaces in contact with the fluids inside the tank	$q_{jac} = \begin{cases} q_{NC}; wet\ surfaces \\ q_{NC} + q_{rad}; dry\ surfaces \end{cases}$
Energy balance in outer surfaces	$q_{jac} + q_{sol} = q_{cc} + q_{rad}$
Heat flow from the sun	$q_{sol} = \begin{cases} [(DNI)sin\theta_{alt} + (DHI)]\alpha_s A; Roof \\ \left[(DNI) \bullet D \bullet Hcos\theta_{alt}\left((DHI) + \rho_{ground}(GHI)\right)\frac{A}{2}\right]\alpha_s; Walls \end{cases}$

tank, though such an investigation falls beyond the scope of this study. Nevertheless, this temperature drop serves as a valuable parameter for conducting subsequent analyses pertaining to the thermal characteristics of analogous molten salt tanks.

In the case of a seasonal thermal energy storage application, the effective operational range of the salts spans from 260 °C to 565 °C. A monthly average temperature loss ranging from 24 °C to 14 °C (worst to best-case scenario as shown Table 4), leads to an round-trip efficiency reduction ranging from 8 % to 5 %. In the case of a seasonal energy storage application for electricity generation, a monthly average temperature loss of 24 °C (Table 4), under the worst-case scenario, implies an efficiency loss in the discharge cycle. The efficiency of a Rankine cycle, which is a thermodynamic cycle used in electricity generation in thermal power plants, is influenced by the temperature difference between the heat source and the heat sink. In this scenario, two different temperatures in the heat sink are being considered, 565 °C and 530 °C.

Generally, a decrease in the temperature of the heat sink (in this case, from 565 °C to 530 °C) tends to reduce the efficiency of the power cycle. This is because the effective temperature difference between the heat source and the heat sink is reduced, diminishing the cycle's ability to convert heat into useful work. While the exact efficiency of the thermal power cycle depends on various factors, including the heat source temperature, heat sink temperature, working fluid properties, and specific cycle design, a baseline case has been considered where only the turbine inlet temperature changes. According to the graph in Fig. 9, this results in a maximum loss of up to 2 % in cycle efficiency in Rankine cycle (blue line) [18]. In this figure, a comparative analysis is conducted on the cycle thermal efficiency and optimal working conditions of three distinct cycles: the air Brayton cycle, s-CO2 Brayton cycle, and steam Rankine cycle, considering various turbine inlet temperatures.

4. Conclusions

This research has demonstrated that molten salt based thermal storage technology has considerable potential to provide long-duration or even seasonal storage for grid applications. The thermal model of

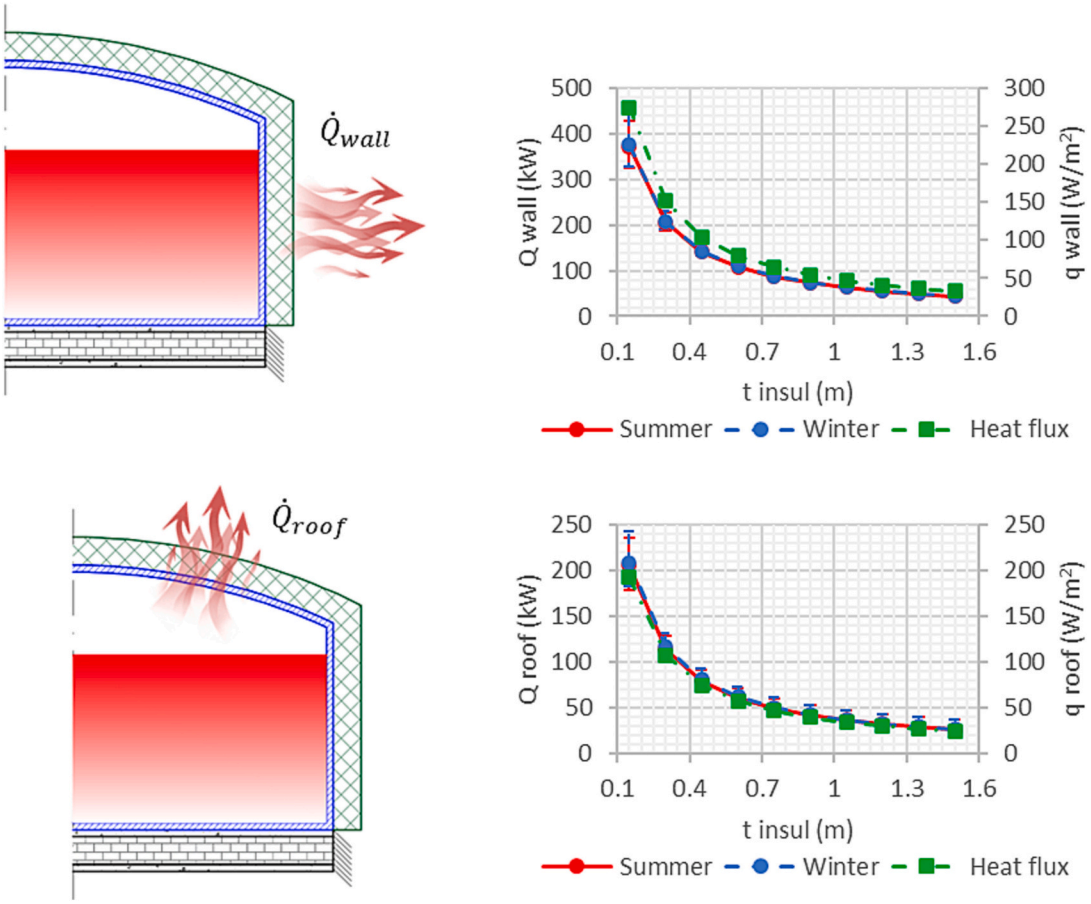

Fig. 6. Calculated heat losses in the molten salt tanks. Top: losses through the walls: losses through the tank roof.

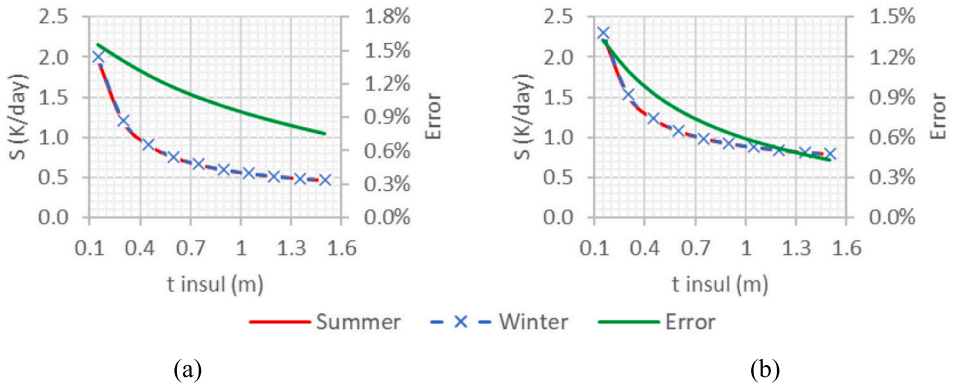

Fig. 7. Results of coefficient C (temperature decrease with time) for (a) a tank not considering local losses, and (b) a tank considering local losses.

Table 4
Temperature drop (in K) in the storage tanks after 30 days at 565 °C.

Insulation thickness (m)	Local losses not considered (K)		Local losses considered (K)	
	Summer	Winter	Summer	Winter
0.15	59.20	60.12	68.42	69.33
0.30	35.92	36.42	45.40	45.89
0.45	27.15	27.50	36.73	37.07
0.60	22.56	22.82	32.18	32.44
0.75	19.73	19.94	29.38	29.59
0.90	17.82	17.99	27.48	27.65
1.05	16.43	16.58	26.11	26.25
1.20	15.38	15.51	25.07	25.19
1.35	14.56	14.68	24.25	24.36
1.50	13.90	14.01	23.59	23.69

Table 5
Results of the calculated thermal losses and the temperature drop.

Parameter	Heat losses (W/m^2)			Cooling rate (K/day)	
	Bottom	Walls	Top	Local losses	No local losses
A	91.9668	−9.9485	−5.8391	0.5314	0.2069
B	−1.5840	59.1639	41.7747	0.3567	0.3589
C	−0.8584	−0.8284	−0.8228	−0.8431	−0.8451
R^2 ($A \neq 0$)	1.000	0.9987	0.9980	1.0000	1.0000
R^2 ($A = 0$)	n.a.	0.9991	0.9994	0.9843	0.9952

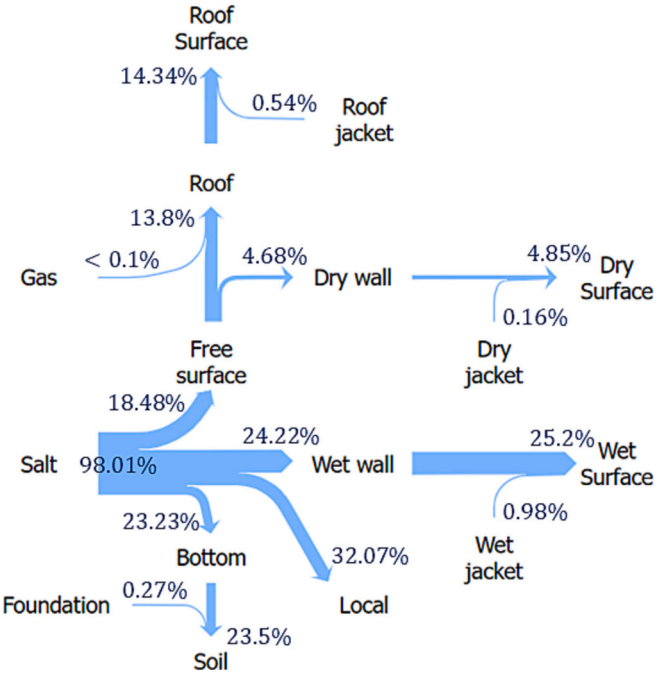

Fig. 8. Heat losses distribution within the tank.

the system illustrates how the insulation system design, and its field assembly process are the relevant factors in ensuring and optimising its economic viability.

A detailed model, which includes the effects of the local heat losses stemming from assembly defects based on real data from pilot molten salt based thermal storage in Seville (Spain) [15] and Lleida (Spain) [16] was developed in a prior work [13]. This model was used to demonstrate how commercial tanks exhibit asymptotic behaviour in their losses for insulation thickness values. The values that were determined were found to be technically and economically feasible in construction. For thicknesses greater than 1.25 m, monthly losses range from 8 % to 5 % between the worst and best construction process scenarios.

The obtained values for monthly losses were found to have broad alignment with the requirements for grid-scale long-duration seasonal storage and underscore the significance of the construction process in enhancing this viability.

Losses in thermal storage systems and their consequent decrease in the temperature of the heat sink has an impact of the thermal-power cycle to discharge the thermal store. The impact on the thermal power cycle has also been analysed, with this impact being less than 2 % in the worst-case scenario.

CRediT authorship contribution statement

Cristina Prieto: Writing – original draft, Validation, Supervision, Methodology, Investigation, Funding acquisition, Formal analysis, Data curation, Conceptualization. **Pablo D. Tagle-Salazar:** Writing – original draft, Software, Methodology, Formal analysis, Data curation. **David Patiño:** Writing – review & editing, Validation, Methodology, Formal analysis, Conceptualization. **Julieta Schallenberg-Rodriguez:** Validation, Formal analysis. **Padraig Lyons:** Writing – review & editing, Validation, Formal analysis. **Luisa F. Cabeza:** Writing – original draft, Methodology, Funding acquisition, Formal analysis, Conceptualization.

Declaration of competing interest

The authors declare that they have no known competing financial interests or personal relationships that could have appeared to influence the work reported in this paper.

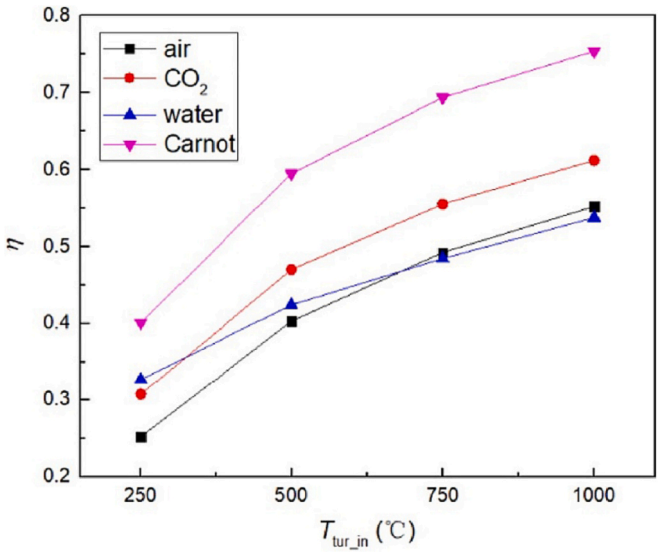

Fig. 9. The maximum cycle thermal efficiency at different turbine inlet temperatures [18].

Data availability

No data was used for the research described in the article.

Acknowledgements

This work was partially funded by the Ministerio de Ciencia e Innovación de España TED2021-132216A-I00 funded by MCIN/AEI/10.13039/501100011033 and the European Union by NextGenerationEU/PRTR. This work was partially funded by the Ministerio de Ciencia e Innovación de España (PID2021-123511OB-C31 - MCIU/AEI/FEDER, UE; RED2022-134219-T). The authors at University of Lleida would like to thank the Catalan Government for the quality accreditation given to their research group GREiA (2021 SGR 01615). GREiA is a certified agent TECNIO in the category of technology developers from the Government of Catalonia. This work is partially supported by ICREA under the ICREA Academia programme.

References

[1] IRENA, Global Energy Transformation: A Roadmap to 2050. https://www.irena.org/publications/2019/Apr/Global-energy-transformation-A-roadmap-to-2050-2019Edition, 2019.

[2] International Energy Agency, Transition to sustainable buildings: Strategies and opportunities to 2050. https://www.iea.org/etp/buildings/, 2013 (accessed February 12, 2019).

[3] International Energy Agency. www.iea.org, 2022 (accessed August 13, 2020).

[4] H. Bahlawan, E. Losi, L. Manservigi, M. Morini, M. Pinelli, P.R. Spina, M. Venturini, Optimization of a renewable energy plant with seasonal energy storage for the transition towards 100% renewable energy supply, renew, Energy 198 (2022) 1296–1306, https://doi.org/10.1016/j.renene.2022.08.126.

[5] M. Child, D. Bogdanov, C. Breyer, The role of storage technologies for the transition to a 100% renewable energy system in Europe, Energy Procedia 155 (2018) 44–60, https://doi.org/10.1016/j.egypro.2018.11.067.

[6] E. González-Roubaud, D. Pérez-Osorio, C. Prieto, Review of commercial thermal energy storage in concentrated solar power plants: steam vs. molten salts, Renew. Sustain. Energy Rev. 80 (2017) 133–148, https://doi.org/10.1016/j.rser.2017.05.084.

[7] IRENA, Innovation Outlook: Thermal Energy Storage, Abu Dhabi, 2020. /-/media/Files/IRENA/Agency/Publication/2020/Nov/IRENA_Innovation_Outlook_TES_2020.pdf?rev=6950b7b9792344b5ab28d58e18209926 (accessed July 7, 2023).

[8] LDES Council, McKinsey & Company, Net-zero heat: Long Duration Energy Storage to accelerate energy system decarbonization, 2022.

[9] S.C. Bhattacharyya, Energy access programmes and sustainable development: a critical review and analysis, Energy Sustain. Dev. 16 (2012) 260–271, https://doi.org/10.1016/j.esd.2012.05.002.

[10] M. Arbabzadeh, R. Sioshansi, J.X. Johnson, G.A. Keoleian, The role of energy storage in deep decarbonization of electricity production, Nat. Commun. 10 (2019) 1–11.

[11] F. Zaversky, J. Garcia-Barberena, M. Sánchez, D. Astrain, Transient molten salt two-tank thermal storage modeling for CSP performance simulations, Solar Energy 93 (2013) 294–311.

[12] A.B. Zavoico, Solar Power Tower Design Basis Document, Revision 0, Albuquerque, NM, and Livermore, CA, 2001, https://doi.org/10.2172/786629.

[13] P.D. Tagle-Salazar, C. Prieto, A. López-Román, L.F. Cabeza, A transient heat losses model for two-tank storage systems with molten salts, Renew. Energy 219 (2023) 119371, https://doi.org/10.1016/j.renene.2023.119371.

[14] P. Fritzson, A. Pop, K. Abdelhak, A. Ashgar, B. Bachmann, W. Braun, D. Bouskela, R. Braun, L. Buffoni, F. Casella, R. Castro, R. Franke, D. Fritzson, M. Gebremedhin, A. Heuermann, B. Lie, A. Mengist, L. Mikelsons, K. Moudgalya, L. Ochel, A. Palanisamy, V. Ruge, W. Schamai, M. Sjölund, B. Thiele, J. Tinnerholm, P. Östlund, The OpenModelica Integrated Environment for Modeling, Simulation, and Model-Based Development, Modeling, Identification and Control: A Norwegian Research Bulletin 41, 2020, pp. 241–295, https://doi.org/10.4173/mic.2020.4.1.

[15] C. Prieto, R. Osuna, A.I. Fernández, L.F. Cabeza, Molten salt facilities, lessons learnt at pilot plant scale to guarantee commercial plants; heat losses evaluation and correction, Renew. Energy 94 (2016) 175–185, https://doi.org/10.1016/j.renene.2016.03.039.

[16] C. Prieto, L. Miró, G. Peiró, E. Oró, A. Gil, L.F. Cabeza, Temperature distribution and heat losses in molten salts tanks for CSP plants, Solar Energy 135 (2016) 518–526, https://doi.org/10.1016/j.solener.2016.06.030.

[17] C. Suárez, F.J. Pino, F. Rosa, J. Guerra, Heat loss from thermal energy storage ventilated tank foundations, Sol. Energy 122 (2015) 783–794, https://doi.org/10.1016/J.SOLENER.2015.09.045.

[18] H. Zhai, S. Wang, B. An, X. Dai, Performance and parameter sensitivity comparison of CSP power cycles under wide solar energy temperature ranges and multiple working conditions, Energ. Conver. Manage. 218 (2020) 112996, https://doi.org/10.1016/j.enconman.2020.112996.